ORIGINAL PAPER

Adhesion Energies

physica status solidi a

www.pss-a.com

Adhesion Energies of 2D Graphene and MoS_2 to Silicon and Metal Substrates

*Jorge Torres, Yisi Zhu, Pei Liu, Seong Chu Lim, and Minhee Yun**

In this paper, results for the adhesion energy of graphene and MoS_2 to silicon based and metal substrates using the intercalation of nanoparticles method are presented. In this method, nanoparticles are dispersed onto the substrates before transferring the 2D material onto the substrate. This causes a blister to form, the width and height of which can be measured by AFM. Using a simple model then allows for the adhesion energy to be found. The substrates tested are SiO_2, Si_3N_4, gold, and platinum. Gold is found to have the highest adhesion energy per area of 7687.10 and 1207.26 mJ m^{-2} for graphene and MoS_2 respectively.

1. Introduction

Two dimensional (2D) materials have recently attracted significant interest due to their unique properties and potential electronic applications. These properties arise because of the confinement of heat transport and charge to a plane as well as due to the material size and shape.[1] Graphene for example has a wealth of excellent characteristics. Some of these characteristics include an intrinsic strength of 130 GPa, an impermeability to gases, a single atom thickness, and excellent flexibility.[2] This wide range of properties has allowed for its use in a wide array of devices, including high frequency transistors,[3] photodetectors,[4] and even batteries.[5] Due to its nanoscopic size, graphene is also being investigated as a replacement for silicon in CMOS devices in order to continue Moore's law.[2] Graphene's success has also sparked research into other 2D materials, such as layered metal oxides and transition metal dichalcogenides (TMDs) such as molybdenum disulfide (MoS_2) and molybdenum telluride ($MoTe_2$). These TMD materials have characteristics that differ from graphene. One difference is that TMDs usually have a band gap which allow them to be used in areas that graphene could not work in while retaining many of the other properties that graphene brings.[1] Due to these excellent qualities, 2D materials have excellent potential to displace currently used materials and processes. However, incorporation of these materials into conventional semiconductor processes such as complementary metal oxide semiconductor (CMOS) processes is a challenge that needs to be overcome in order to facilitate inclusion of 2D materials as rapidly as possible.

The processes needed to develop devices with 2D materials differ slightly from conventional CMOS processes. In conventional CMOS fabrication processes, a thin film is grown directly on the substrate via chemical vapor deposition (CVD) or electron-beam (e-beam) evaporation processes and then patterned. For example, polysilicon can be grown via CVD through the use of high temperatures and low pressure which yields a uniform film thickness.[6] Most metal contacts are often grown with e-beam evaporation due to the directionality and the ability to have a uniform thin film. However, 2D materials often cannot be grown directly on the desired substrates, especially in the case of non-metallic substrates.[2] Therefore, the 2D materials need to be grown on another substrate and then physically transferred onto the target substrate. Device performance and functionality may be compromised by this physical transfer process. For example, graphene is known to change properties depending on what surface it is on.[7] There are many methods of transferring 2D materials based on how they were grown, two of which are mechanical exfoliation from a layered material or a wet transfer process from 2D materials grown via CVD. In mechanical exfoliation, scotch tape can be used with a layered material and rubbed against a photoresist in order to leave behind a variety of flakes on the photoresist surface which can then be transferred to the desired substrate. For the wet transfer process, a CVD process is used to grow the 2D material on a substrate. The material is then covered with a polymer and set in a chemical bath to etch away the substrate. After cleaning by transferring the polymer/2D material hybrid into DI water, it can then be transferred onto the target substrate which will degrade the adhesion between the substrate and the 2D material as compared to conventional thin film technology.[1] The polymer

J. Torres, Prof. M. Yun, P. Liu
Department of Electrical and Computer Engineering
University of Pittsburgh
Pittsburgh, PA 15261, USA
E-mail: miy16@pitt.edu

Y. Zhu
Materials Science Division
Argonne National Lab
Lemont, IL 60439, USA

Prof. S. C. Lim
Department of Energy Science
Sungkyunkwan University (SKKU)
Suwon 16419, Korea

Prof. S. C. Lim
Center for Integrated Nanostructure Physics
Institute for Basic Science (IBS)
Suwon 16419, Republic of Korea

The ORCID identification number(s) for the author(s) of this article can be found under https://doi.org/10.1002/pssa.201700512.

DOI: 10.1002/pssa.201700512

can then be removed with acetone, which may leave behind residues that may also affect device performance. Hence, the performance of advanced electronic devices with 2D materials depends strongly on the transfer process providing a strong and clean adhesion.

Surface forces determine the strength of the adhesion energy between two materials and are a key factor in determining device functionality. Due to their increased surface area to volume ratio, 2D materials are often more strongly affected by surface interactions than other materials. These surface interactions have been reported to cause Fermi-level pinning by metals on MoS2,[8] reduced electron mobility in graphene on SiO_2,[9] bandgap opening in graphene from SiC,[10] among many other effects. Additionally, transfer processes can suffer from polymer contamination that can degrade material performance.[2] Since 2D materials are very attractive, it is essential to understand how they adhere to substrates so that sustainable and reliable device processes can be developed. A major force for substrate adhesion is the van der Waals force, consisting of the Keesom force, the Debye force, and the London dispersion force.[11] The London dispersion force is often the major force at play and is a result of two instantaneously induced dipoles acting on each other. The force becomes stronger in two ways. The first way is through an increase in the atomic radius due to the increased polarizability of larger, more dispersed electron clouds. The second way is through an increase in the contact surface area which results in more intermolecular interactions. Because 2D materials can be highly conformative, a non-planar surface may significantly increase the actual surface area and therefore cause a higher adhesion energy if not accounted for.[9] These factors have an influence on the strength of the London dispersion force which in turn affects the strength of the adhesion energy. By investigating the adhesion mechanics between 2D materials and other substrates via understanding of the surface forces at play, it will be possible to increase the understanding of growth mechanisms, transfer processes, and material properties, especially in regards to how they change due to substrate interactions, leading to an improvement in device performance.

Investigations into adhesion energy are thus influenced by the strength of the London dispersion force. Previous investigations into the adhesion properties between graphene and various substrates have been made. Yoon et al. used a double cantilever test to measure the adhesion of as grown graphene to copper and obtained an adhesion energy of $0.72\ J\ m^{-2}$.[12] Additionally, Li et al. used the Density Functional Theory model to gain an adsorption energy of graphene to copper in which the adhesion energy and the binding energy was contained. By subtracting the binding energy from the adsorption energy, the adhesion energy was found to be $2483\ mJ\ m^{-2}$.[13] Das et al. used a nanoscratch method to find the adhesion energy of graphene to copper and nickel, finding the energy to be 12.8 and $72.7\ J\ m^{-2}$ respectively.[7] Koenig et al. used a pressurized blister test with graphene sheets on a SiO_2 substrate and recorded an adhesion energy of $0.31\ J\ m^{-2}$ for few layer graphene.[14] In Zong et al., the adhesion of graphene to SiO_2 was found by using an intercalation of nanoparticles method which found an adhesion energy of $0.151\ J\ m^{-2}$ for few layer graphene. While there have been many investigations into the adhesion energy of graphene, more work still needs to be done to fully explore this area as well as that of other 2D materials.

In this report, we have investigated van der Waals interaction on various substrates of gate dielectrics and metal electrodes including, SiO_2, Si_3N_4, Au, and Pt, for the adhesion properties of graphene and MoS_2. The intercalation of nanoparticles method will be employed, using gold nanoparticles as the supports. This method drops a nanoparticle solution on the surface of a substrate before transferring the 2D material. These nanoparticles then act as wedges between the 2D material and the substrate, creating blisters in the process. The blisters are where the 2D material does not touch the surface of the substrate. The thickness of the 2D layer, the blister height, and the blister radius can then all be measured and used to calculate the adhesion energy to the substrate. The method's several advantages are that it is a relatively cheap and easy method to perform, can be done with any suitable particle, and it is free from edge effects.[15] We believe this work would help to overcome a lack of understanding adhesion characteristics for MoS_2 as well as adding to the knowledge of graphene adhesion properties to various substrates.

2. Experimental Section

Figure 1 illustrates the sample preparation process. The process begins with 2D layer growth and transfers this layer onto a substrate. The substrate was separately prepared to have nanoparticles coating the surface before the 2D layer was transferred on top. Since both graphene and MoS_2 were studied, two growth and transfer processes were necessary.

Growing graphene was accomplished through the use of a Cu substrate (Figure 1a). The Cu substrate was 0.025 mm thick and 99.8% pure on a metals basis (Alfa Aesar). The substrate was cleaned with acetone and IPA and dried via hot plate. A CVD process was employed to grow graphene on the Cu surface. First, the chamber was purged by running Ar and H_2 gas through the chamber before raising the temperature to 1000 °C over 30 min. This was then followed by annealing at 1000°C for 30 min. After the annealing process, CH_4 was also run through the chamber for 10 min, after which the chamber was allowed to cool. This process produced a few layers of graphene, as determined by AFM measurements of the graphene thickness on SiO_2, on top of the copper surface (Figure 1b). After the graphene was grown, it was transferred onto the substrates. This was accomplished by spin coating PMMA 495 A2 onto the graphene side of the Cu (Figure 1c). The backside of the Cu was cleaned by oxygen plasma for 10s. These Cu/graphene pieces were cut to size in order to fit onto the previously prepared substrates with nanoparticles. The underlying copper was etched by an ammonium persulfate (APS) solution overnight (Figure 1d). The remaining graphene/PMMA pieces were then transferred to DI water three times for 10 min to reduce contamination (Figure 1e). Afterwards, the graphene was transferred onto the sample pieces and left to dry in ambient overnight. Finally, the PMMA was removed by leaving the samples in acetone for 30 min, followed by IPA for 5 min and then left to dry in ambient.

The MoS_2 layers were also grown via a CVD process as shown in Han et al, using SiO_2 as a substrate layer.[16] SiO_2 was coated

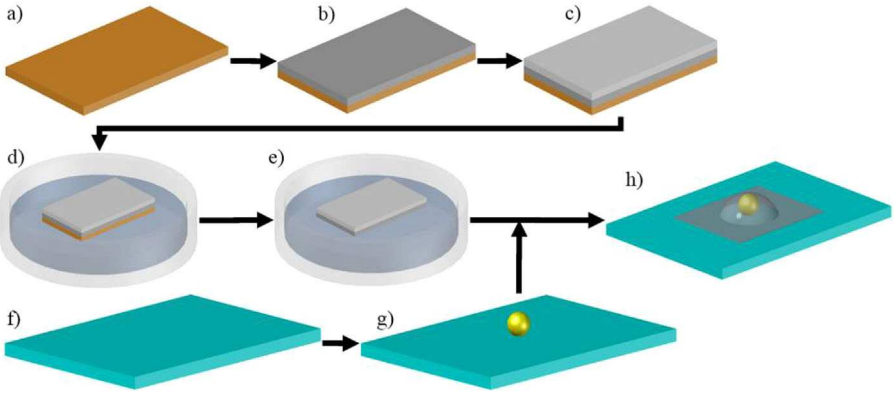

Figure 1. The substrate creation process. a) A growth substrate is chosen and cleaned. b) The 2D material is grown on the substrate using a CVD method. c) PMMA is spun on top of the 2D material and the backside of the substrate is cleaned of any excess 2D material growth. d) The prepared substrate is put into an etchant bath. e) The substrate is etched away and the remaining 2D material and PMMA hybrid is cleaned. f) A substrate is chosen to deposit nanoparticles onto. g) Gold nanoparticles are deposited onto the substrate. h) The 2D material is transferred onto the prepared substrate, sandwiching the nanoparticle in between the substrate and the 2D material and creating a blister.

with MoO_3 seed particles and further processed to improve MoS_2 quality. It was then placed into a CVD furnace with solid Sulphur on the upstream end (Figure 1a). A nitrogen flow of 700 sccm was introduced and the temperature was ramped to 750 °C. The MoS_2 layer was grown for 20 min and then the sample was rapidly cooled to room temperature (Figure 1b). These samples were cut to size before spin coating with PMMA (Figure 1c). The SiO_2 was etched away by a dilute HF and DI water solution (Figure 1d). This allowed the MoS_2 to detach from the SiO_2 and remain floating while the remaining Si piece sank. As with graphene, the MoS_2 layers were transferred to DI water baths in order to clean the samples of acid and reduce contamination (Figure 1e). After this, the MoS_2 was transferred onto the substrate and left to dry in ambient. The PMMA was removed by leaving the samples in acetone for 30 min, followed by being in IPA for 5 min and left to dry in ambient.

The substrate preparation process was done parallel to the 2D layer process. Samples were prepared on Si_3N_4 and SiO_2 wafers. SiO_2 was grown using thermal wet oxidation and SiN was grown using a low stress LPCVD method. The thickness of the SiO_2 layer of the SiO_2 wafers was 100 nm while the thickness of the nitride layer of the Si_3N_4 wafers was 1 micron. These wafers were cut into rectangular pieces a few centimeters a side. The pieces were then cleaned with acetone and IPA before being rinsed with DI water and dried via heating on a hot plate. Gold and Pt layers were created using an electron-beam (e-beam) evaporator. The Au layers were 30 nm thick, while the Pt layers were 11 nm thick (Figure 1f). After substrate creation, the samples were coated with Au nanoparticles with a 50 nm diameter, supplied in a sodium citrate solution (Alfa Aesar). A diluted form of the solution was created in a separate beaker by adding DI water to the nanoparticle solution at a ratio of 9:2 DI: Nanoparticle solution. This dilute solution of nanoparticles was then dropped onto the samples and then left to dry overnight in ambient conditions (Figure 1g). The dilution was performed in order to reduce clustering of the nanoparticles, though such clustering was unavoidable. Once the samples had dried, 2D layer transfer was performed. This allowed for the 2D layer to lie on top of the nanoparticles (Figure 1h).

Samples created by the above processes resulted in a 2D material bound to the substrates by surface forces, such as the van der Waals forces, but had nanoparticles acting as supports which created a blister in the 2D material. The blister is an area where the 2D material is not in contact with the substrate. The area of the blister will depend on the actual size of the nanoparticle, with larger nanoparticles causing a larger blister to appear. The size of the blister can then be used to determine the adhesion energy between the 2D material and the substrate.

Characterization of the adhesion energy was performed by using an SEM (Zeiss Sigma 500VP) and an AFM in tapping mode. The SEM was used to find areas where good blisters developed. These good blisters are where a single nanoparticle was the support of a circular blister. This blister was then measured with AFM. The AFM was also used to find the thickness, and therefore the number of layers, of the 2D material. The AFM measurements were made using tapping mode, with a scan area that was 5um by 5um and a 400×400 pixel resolution. The thickness measurements were made on SiO_2 for both 2D materials. The adhesion energy was then extracted by inputting the data into a model.

Modeling of the blister began through the consideration of a thin plate with an external load (P) produced by a central shaft of radius (R) as in Wan et al. This leads to the formation of a blister with radius, a (where $a >> R$), and central deflection $w_0 = \frac{3(1-\nu^2)Pa^2}{4\pi}$ with v as the Poisson's ratio of the membrane. When the blister is loaded, one is able to find the mechanical energy release rate. However, the use of this formulation is not yet sufficient due to three reasons: (i) the model only accounts for the bending mode which doesn't account for the dominant stretching mode in thin membranes, (ii) the point contact at the center of the blister leads to an unphysical stress singularity, (iii) plastic yielding in the area near the blister is not accounted for.[17]

Therefore, a thin flexible membrane must be considered under the same loading conditions as the thin plate. This

includes the assumption that the radius a >> R. They first considered the elastic response by defining the tangential and radial strains and stresses. This allowed the researchers to obtain[17]

$$\frac{d}{dr}\left(\nabla^2 f\right) + \frac{Eh}{r}\left(\frac{dw}{dr}\right)^2 = 0 \quad (1)$$

where f is the stress function defining the radial and tangential stresses, E the Young's modulus, and h the thickness of the thin plate. By using the principle of virtual work, the researchers were then able to establish a load function. An energy balance according to linear elastic fracture mechanics was able to be derived by also considering the blister profile. At equilibrium, the interfacial energy of the membrane adhered to the substrate, W, becomes[17]

$$W \approx \frac{Eh}{32k_{el}}\left(\frac{w_0}{a}\right)^4 \quad (2)$$

where k_{el} is a slowly varying function of a for small debonding angles <25°. This equation is valid as long as the effective stress stays below the yielding strength, which allows the blister to remain elastic. The stress approximations used are also not valid inside the contact circle (r < a), however when P is small, the contact zone contribution is negligible.[17]

Furthermore, for this experiment a nanoparticle will be used instead of a central shaft. For small debonding angles, $k_{el} \approx 1/2$. This allowed Zong et al to write the equation as[15,17]

$$\gamma = \lambda Eh\left(\frac{w}{a}\right)^4 \quad (3)$$

where λ is a geometrical factor =1/16 for a circular blister and comes from $\frac{1}{32k_{el}}$ and w takes the place of w_0. Therefore, Eq. (3) is simply Eq. (2) rewritten for simplicity. In the creation of this equation, some other assumptions have been made. The first assumption is that the 2D layer behaves as a flexible membrane with negligible flexural rigidity because w and a are much greater than h. The second is that the substrate and support particle are taken to be rigid with negligible deformation. This is justified because the 2D layers are ultrathin and because as long as the wedge can support the load and does not collapse the minor correction to the equation is negligible.[15] A visualization of the parameters given in Eq. (3) is shown in **Figure 2**. Figure 2a shows the diameter of the blister, 2a, in a 3D perspective, while Figure 2b shows a cutout side view of the blister. Figure 2b additionally shows the height of the 2D material, h, and the height of the blister, w. The gold sphere represents the nanoparticle, while the gray layer represents the 2D blister it creates.

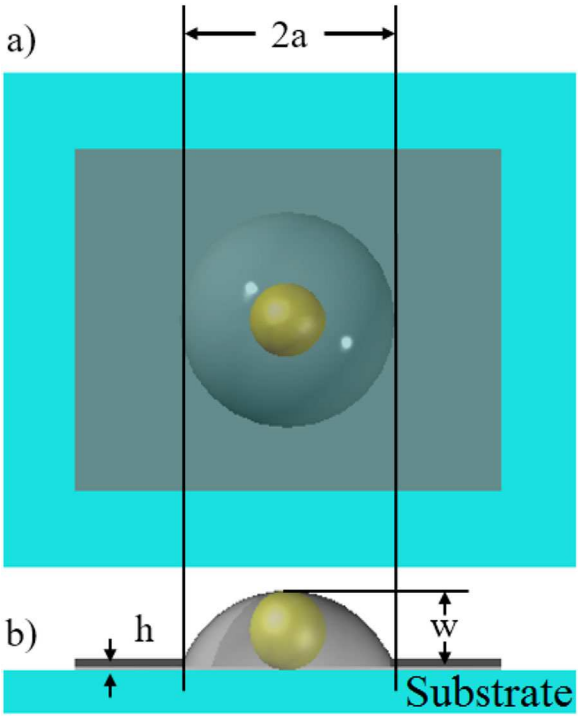

Figure 2. A representation of the parameters in (3). h is the thickness of the 2D material, a is the radius of the blister, w is the height of the blister. a) a top view, b) a cross sectional representation.

3. Results and Discussion

Figure 3 shows an SEM with nanoparticles and graphene blisters on a SiN substrate. As expected, there are regions of both individual nanoparticles, position A, and of multiple nanoparticles, position B, which created more complex blisters. Additionally, one can see the wrinkling of the graphene layers in the SEM image, position C, likely due to the transfer process as the graphene may not have been transferred perfectly flat. This wrinkling effect was also seen in the MoS_2 samples for the same reason. AFM measurements were made using blisters like those in position A.

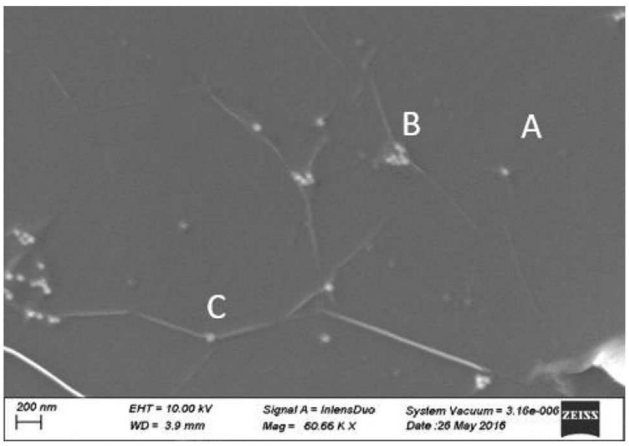

Figure 3. SEM image of graphene on SiN with gold nanoparticles taken at a working distance of 3.9 mm and a magnification of 60.66kx. The electron beam was held at 10 kV. Position A shows a regular blister with a single nanoparticle. Position B shows a complex blister with many nanoparticles. Position C shows a single nanoparticle blister with a wrinkle in the graphene layer.

AFM imaging was done via tapping mode in order to obtain the graphene blister profiles as seen in **Figure 4**. The graphene thickness was measured to be 3.4 nm, corresponding to several layers of graphene. The sample was scanned for $5 \times 5um^2$ size images with a 400×400 pixel resolution. The AFM software allowed for the blister height (w) and the blister diameter (2a) to be measured accurately by taking the lowest points of the line profile to be the contact point between graphene and the substrate. This AFM scanning process was done for graphene on SiO_2, SiN, Au, and Pt. Figure 4 shows a sample AFM image of graphene on top of (a) a SiO_2 substrate and (b) a platinum substrate along with their associated line profiles. The height of the substrate and blisters can be determined by the color of the images. The bright circular region indicates the blister that was measured, showing both its height and its diameter. The height and width of the blister in Figure 4a were found to be 24 and 260 nm while for Figure 4b they were 31 and 190 nm respectively. The adhesion energies were found to be 739.2 and 2409.41 mJ m^{-2} for Figure 4a and b respectively.

The same AFM imaging process was repeated for MoS_2 as seen in **Figure 5**. The thickness for MoS_2 was found to be 1.4 nm, indicating 2–3 layers of MoS_2. Figure 5 shows sample scanned images for (a) SiO_2, (b) SiN, (c) gold, (d) and platinum along with their associated line profiles. As before, the colors represent the height measured by the AFM with the brighter colors representing taller features. This again allowed the blister diameter to be easily determined. The adhesion energies for Figure 5a–d were found to be 344.24, 571.01, 1219.53, and 631.87 mJ m^{-2} respectively.

The blister heights (w) and blister diameters (2a) were measured from the AFM images and analyzed. **Figure 6** shows the range of these two parameters for (a) graphene and (b) MoS_2. The red data points indicate the blister height, w, while the blue data points indicate the blister diameter, 2a. The bars show the min and max values obtained while the boxes show the range of the middle 50% of the data. It was expected that the heights of the blisters would be near 50 nm due to the use of 50 nm diameter nanoparticles. This was found not to be the case. There are two explanations for this: (i) the 50 nm figure is only the average nanoparticle size and there is actually a small range of nanoparticle sizes; (ii) the nanoparticles collapsed or were otherwise distorted. In either case, the different sizes will not affect the resulting measurements as long as the nanoparticle is acting as a support since Eq. (3) does not expect a certain blister height or blister diameter. Additionally, since the profile of each measurement was similar, the cases where the nanoparticle was much smaller than expected still give good data. Additionally, from the data in Figure 6 we can get an idea of which material is more strongly adhered. Since the adhesion energy is proportional to $\left(\frac{w}{a}\right)^4$, it can be seen that situations where the diameter is lower on the graph than its corresponding height corresponds to higher adhesion energies. This observation is borne out by the final results.

The results shown in Figure 6 were then put into (3) to get the average adhesion energy for each 2D material and substrate combination. The Young's modulus of the 2D material is also needed to get the adhesion energy. The Young's modulus of graphene was taken to be 1TPa, as recently reported,[18] while the Young's modulus of MoS_2 was taken to be 0.33TPa.[19] The results for the average adhesion energies of the 2D materials on each substrate are given in **Table 1**. Table 1 shows that graphene is overall more strongly bonded to the substrate than MoS_2, while both 2D materials most strongly bond with gold. Additionally, the result for graphene and SiO_2 corresponds well with other experiments in that once the thickness difference is accounted for, the experiments and this work measure similar quantities for the adhesion energy.[15,20] Differences between the results have a few possible causes: (i) the samples were not measured in a vacuum which causes the blister radius to be smaller; (ii) moisture from the transfer process may be stuck in between the membrane and the substrate which would cause the

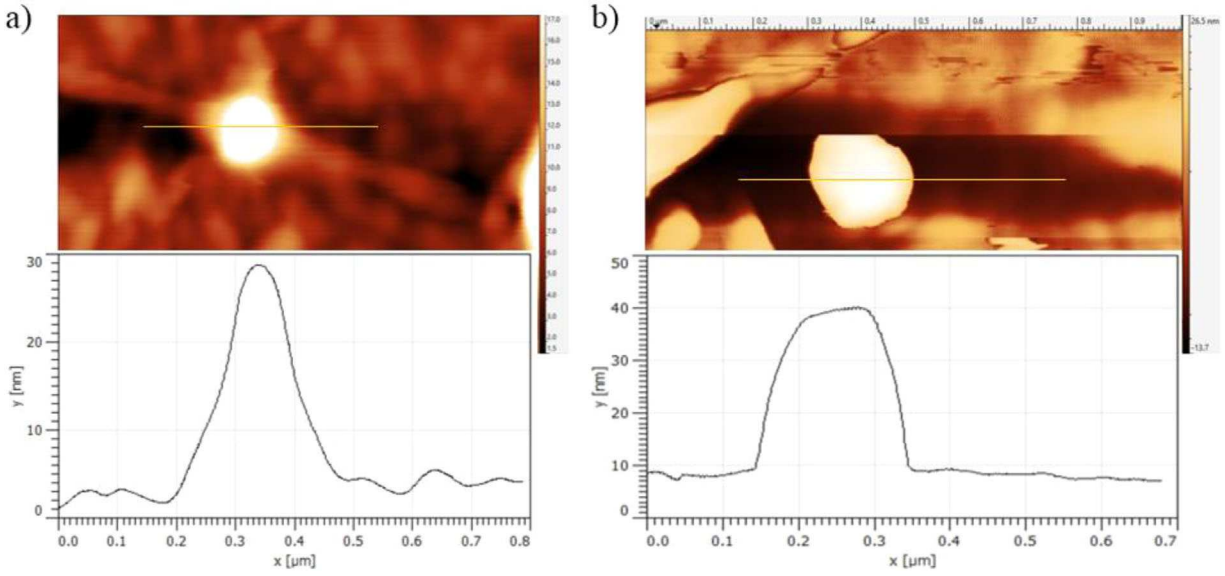

Figure 4. Sample AFM images of graphene covering a gold nanoparticle on top of (a) a SiO_2 substrate, (b) a platinum substrate. The lighter regions represent taller structures. The associated line profiles taken from each blister are also shown. The x-direction is in um and the y-direction is in nm.

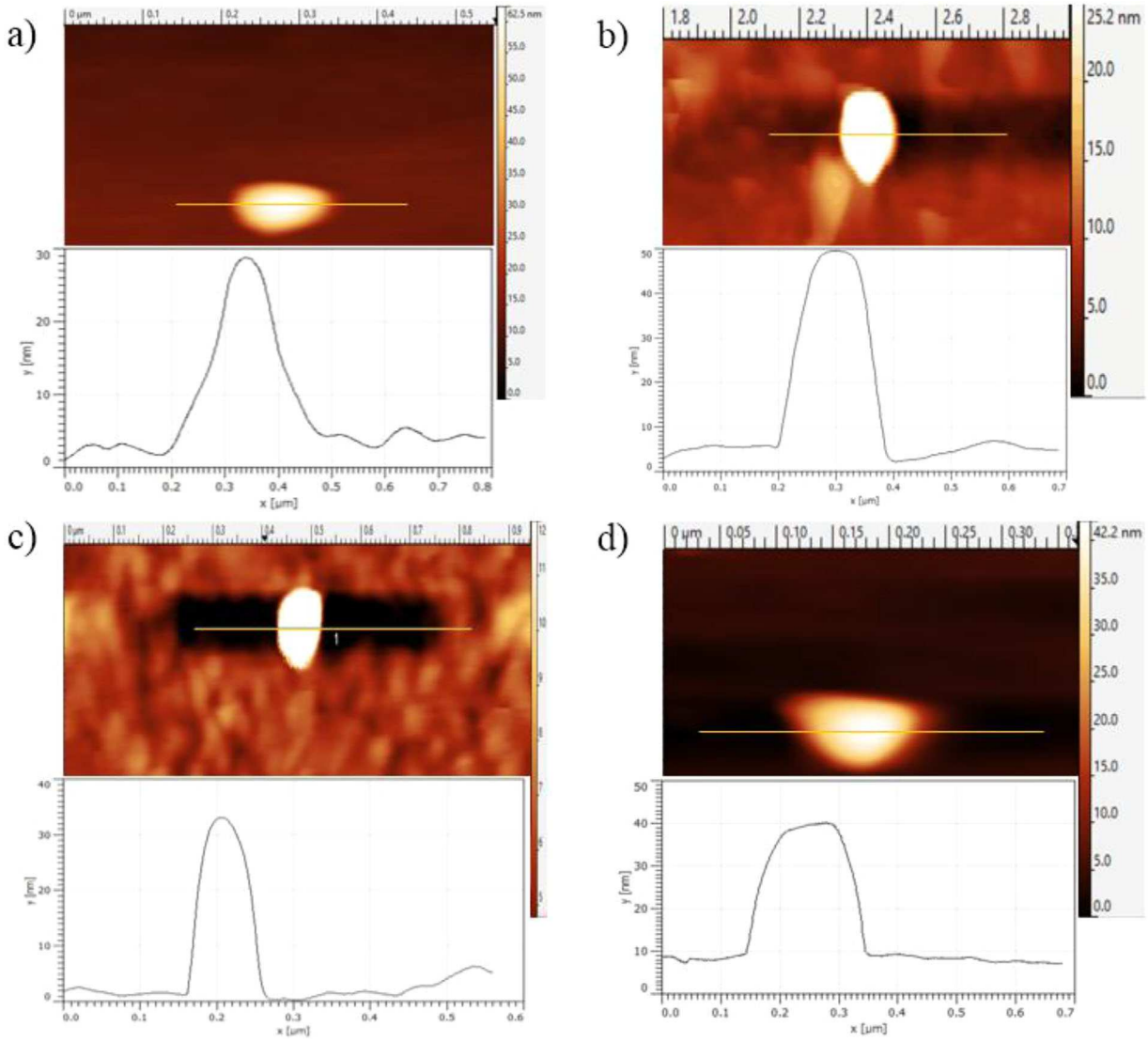

Figure 5. Sample AFM images of MoS_2 covering a gold nanoparticle on top of (a) a SiO_2 substrate, (b) a SiN substrate, (c) a gold substrate, and (d) a platinum substrate.

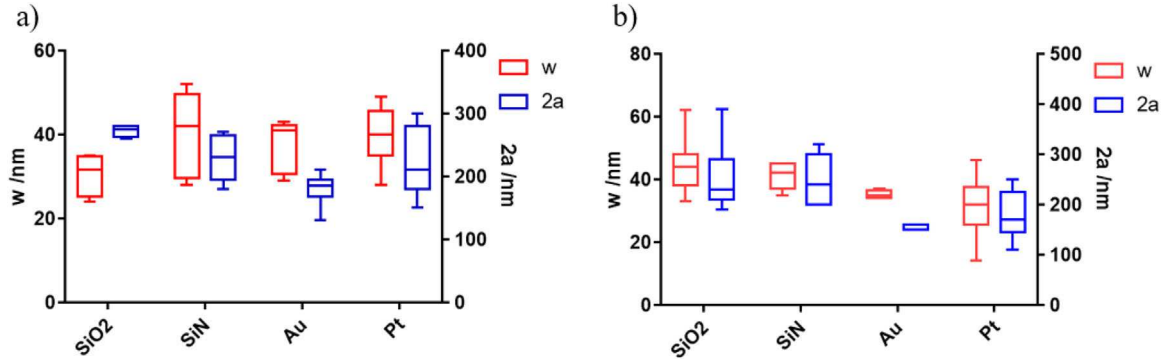

Figure 6. Blister data for (a) Graphene and (b) MoS_2. The data on the left for each substrate corresponds to "w," where w is the blister height, while the data on the right corresponds to "2a," where a is the blister radius.

Table 1. Adhesion energies for Graphene and MoS_2 samples for their respective substrates.

Substrate	Graphene [mJ m^{-2}]	MoS_2 [mJ m^{-2}]
SiO_2	567.14	482.48
SiN	3281.64	429.00
Au thin film	7687.10	1207.26
Pt thin film	4021.47	690.64

blister radius to appear larger. Since the adhesion energy of graphene is comparable to other results, the process was determined to create a sufficiently dry sample. The same drying process was used for the MoS_2 samples and therefore are also sufficiently dry.

Graphene was found to be more strongly bound to the substrates than MoS_2. This can be explained through an examination of Eq. (3). If graphene and MoS_2 adhere to the substrates in a similar manner, that is, that the ratio between the blister height and the blister radius is about the same, then the only remaining factors that can cause a difference in the adhesion energy are the Young's modulus and the thickness of the 2D material. The Young's modulus for graphene is roughly three times bigger than that of MoS_2, and the graphene sample was roughly twice as thick. Therefore, assuming that the blisters retain the same height to radius ratio, it is expected that the adhesion energy for graphene is about six times larger than that for MoS_2. This is the case for Si_3N_4, Au, and Pt substrates, for which graphene has a larger adhesion energy than MoS_2 by roughly 7.6, 6.4, and 5.8 times respectively. However, graphene and MoS_2 had very similar adhesion energies for SiO_2 which points to an increased interaction between MoS_2 and SiO_2.

Unexpectedly high adhesion energies were obtained for MoS_2 on the SiO_2 substrate. Due to the differences in Young's modulus and material thickness, as explained above, MoS_2 was expected to have an adhesion energy on SiO_2 less than 100 mJ m^{-2}. The adhesion energy was much higher than this, being 482.48 mJ m^{-2} instead. It is thought that the sulfur and oxygen atoms in the respective materials have an increased interfacial bonding than would be expected through a normal van der Waals force. Indeed, organic chemists have known of this interaction for some time as it occurs in heteroaromatic rings with a sulfur atom interacting with the oxygen atom of another molecule. The complex interactions in the ring result in the sulfur atom achieving a positive charge while the oxygen retains a negative charge and thus results in a more strongly bonded adhesion than would normally be expected.[21] For MoS_2, this redistribution of charge would likely have to occur through the 2D materials extensive double bond network which can serve as a mechanism for redistributing charge and causing this increased interaction. Additional modeling is needed in order to determine if this is the true cause of the stronger than expected adhesion energy. Additionally, this interaction results in the adhesion energy for MoS_2 being slightly stronger for the SiO_2 substrate than for the SiN substrate, which is contrary to what was expected given the outcome of the graphene results.

Both 2D materials were most strongly bound to the gold substrate as shown in Table 1. The specific forces acting on the materials is not explicitly expressed by Eq. (3) as the equation only takes some physical parameters to find the adhesion energy. However, it is well known that van der Waals forces act on all materials and thus are an influencing factor on the adhesion energy. The London dispersion force is usually the most significant of these forces and its strength is proportional to the polarizability of the two materials.[22] The polarizability of gold is much larger than that of SiO_2 or Si_3N_4. This indicates that the London dispersion force will be much greater for gold than the other substrates and therefore the adhesion energy will be larger. The London dispersion force being larger would manifest itself in (3) as a larger w/a ratio as the increased adhesion forces would result in a smaller blister radius for a given blister height. It is this mechanism that results in a stronger adhesion energy for gold than for either SiO_2 or Si_3N_4.

The results show that the Young's modulus has a big impact on the adhesion energy of a given 2D material for a given thickness. The higher a material's Young's modulus, the higher the expected adhesion energy and thus the better device reliability that can be expected. In this case, graphene based devices are expected to be more reliable than MoS_2 based devices. However, this does not preclude MoS_2 devices from being reliable. In the case of SiO_2, MoS_2 devices can actually be expected to have similar reliability characteristics as in graphene devices.

4. Conclusion

We reported on the adhesion energies of graphene and MoS_2 on various substrates using the intercalation of nanoparticles method in order to gauge device reliability and aid in design of devices that incorporate 2D materials. It was shown that graphene was more strongly adhered to the substrates than MoS_2 due to its higher Young's modulus. This shows that materials with higher Young's modulus will in general adhere better to a substrate for a given thickness, though such an advantage can be overcome due to other particle interactions as seen with the higher than expected adhesion energy between MoS_2 and SiO_2. We stipulate that this is due to an increased positive charge on the Sulfur atoms of MoS_2 interacting with the negative charge of the oxygen atoms in SiO_2. The adhesion energy for both graphene and MoS_2 was strongest on gold with an adhesion energy of 7687.10 and 1207.26 mJ m^{-2} respectively.

Acknowledgements

The authors are grateful to the National Science Foundation (NSF) for the financial support from NSF ECCS 1709307 and the support from NSF HRD 1434012 for this research.

Conflict of Interest

The authors declare no conflict of interest.

Keywords

adhesion, graphene, MoS_2

Received: July 21, 2017
Revised: October 30, 2017
Published online: December 15, 2017

[1] A. Gupta, T. Sakthivel, S. Seal, *Prog. Mater. Sci.* **2015**, *73*, 44.
[2] A. C. Ferrari, F. Bonaccorso, V. Fal'Ko, K. S. Novoselov, S. Roche, P. Bøggild, S. Borini, F. H. Koppens, V. Palermo, N. Pugno, J. A. Garrido, *Nanoscale* **2015**, *7*, 4598.
[3] Z. Guo, R. Dong, P. S. Chakraborty, N. Lourenco, J. Palmer, Y. Hu, M. Ruan, J. Hankinson, J. Kunc, J. D. Cressler, C. Berger, *Nano Lett.* **2013**, *13.3*, 942.
[4] A. Urich, K. Unterrainer, T. Mueller, *Nano Lett.* **2011**, *11.7*, 2804.
[5] E. J. Yoo, J. Kim, E. Hosono, H. Zhou, T. Kudo, I. Honma, *Nano Lett.* **2008**, *8.8*, 2277.
[6] H. Kurokawa, *J. Electrochem. Soc.* **1982**, *129.11*, 2620.
[7] S. Das, D. Lahiri, D. Y. Lee, A. Agarwal, W. Choi, *Carbon* **2013**, *59*, 121.
[8] C. Gong, L. Colombo, R. M. Wallace, K. Cho, *Nano Lett.* **2014**, *14*, 1714.
[9] S. Fratini, F. Guinea, *Phys. Rev. B.* **2008**, *77*, 195415.
[10] S. Y. Zhou, G. H. Gweon, A. V. Fedorov, P. N. First, W. A. De Heer, D. H. Lee, F. Guinea, A. C. Neto, A. Lanzara, *Nat. Mater.* **2007**, *6*, 770.
[11] Z. Lu, M. L. Dunn, *J. Appl. Phys.* **2010**, *107.4*, 044301.
[12] T. Yoon, W. C. Shin, T. Y. Kim, J. H. Mun, T. S. Kim, B. J. Cho, *Nano Lett.* **2012**, *12.3*, 1448.
[13] Y. Li, M. Li, T. Wang, F. Bai, Y. X. Yu, *Phys. Chem. Chem. Phys.* **2014**, *16*, 5213.
[14] S. P. Koenig, N. G. Boddeti, M. L. Dunn, J. S. Bunch, *Nat. Nanotechnol.* **2011**, *6.9*, 543.
[15] Z. Zong, C. L. Chen, M. R. Dokmeci, K. Wan, *J. Appl. Phys.* **2010**, *107.2*, 026104.
[16] G. H. Han, N. J. Kybert, C. H. Naylor, B. S. Lee, J. Ping, J. H. Park, J. Kang, S. Y. Lee, Y. H. Lee, R. Agarwal, A. C. Johnson, *Nat. Commun.* **2015**, *6*, 6128.
[17] K. T. Wan, Y. W. Mai, *Int. J. Fract.* **1996**, *74.2*, 181.
[18] Z. Cao, P. Wang, W. Gao, L. Tao, J. W. Suk, R. S. Ruoff, D. Akinwande, R. Huang, K. M. Liechti, *Carbon* **2014**, *69*, 390.
[19] A. Castellanos-Gomez, M. Poot, G. A. Steele, H. S. van der Zant, N. Agraït, G. Rubio-Bollinger, *Adv. Mater. (Weinheim, Ger.)* **2012**, *24.6*, 772.
[20] J. S. Bunch, M. L. Dunn, *Solid State Commun.* **2012**, *152.15*, 1359.
[21] X. Zhang, Z. Gong, J. Li, T. Lu, *J. Chem. Inf. Model.* **2015**, *55*, 2138.
[22] J. N. Israelachvili, *Intermolecular and Surface Forces*, Elsevier Academic, Amsterdam, NL **2011**.